ute to the amount of tethered chain between the PS and the network. First, the chain will pull out of the network and remain on the substrate until the penetrated length reduces to the size of the relaxed plume, which acts as an anchor. As the plume decreases in size with increasing slip speed, the fraction of the tethered chain on the substrate will increase with slip speed. Second, the kinetics of the penetration of an end-grafted chain into a network, which has been studied theoretically (*17*) and by simulation (*18*), will have an effect. Initially, penetration is very rapid until the patch of chain on the substrate (between the tether point and the point of entry to the network) becomes stretched. However, complete penetration is a very slow process, and it is reasonable that it might not occur in the time scales observed here, about 0.5×10^{-3} s.

At low speeds, the 2.4-nm layer showed friction similar to that of the 0-nm and 1.2-nm layers but much lower friction at high speeds. Presumably, much of the tethered chains can again penetrate the network at low speeds, but a slip speed of only about 1 $\mu m\ s^{-1}$ is required to start forming a layer of the tethered chains on the PS. For the 5.6-nm layer, the friction was reduced from that observed for the 2.4-nm layer over the whole experimentally accessible speed range. The shear stress at the lowest observable velocity, 0.01 $\mu m\ s^{-1}$, was reduced by a factor of 2. The measurements were not taken over a long enough time scale to test for the existence of a finite shear stress as the velocity tended to 0, but none of the thinner layers showed linear, viscous-like slip at low velocities. Compared to the 5.6-nm layer, the 9.2-nm layer showed only a small decrease in shear stress at high velocity but at low velocity showed a considerable decrease in shear stress so that the stress apparently tended to 0 at 0 velocity. Hence, the slip showed liquid-like characteristics. Presumably, the network chains did not contact the PS.

It is valuable to consider the absolute values of the shear stress observed with the 9.2-nm layer, as the slip appeared to show liquid-like properties at low velocities. At the lowest stresses, the shear stress varies approximately linearly with the slip rate with a gradient (slip coefficient) of about 2×10^{10} Pa·s m^{-1}. A simple lower bound estimate for the slip coefficient would be $\zeta_1 a^{-2}$, where ζ_1 is the monomer friction coefficient (*19*) and a is a monomer size. This value might be observed between PDMS layers that show no penetration. Assuming $a = 0.48$ nm and $\zeta_1 = 8.9 \times 10^{-12}$ N·s m^{-1}, this lower bound value for the slip coefficient is 3.7×10^7 Pa·s m^{-1}, much lower than that observed. Clearly there is some penetration between the end-tethered layer and the network. The slip coefficient can also be compared with the value expected if the chains penetrated the network fully, but the friction was just simple segmental friction rather than the enhanced friction predicted by Ajdari, Rubinstein, and co-workers. These simple segmental friction assumptions give a coefficient of $\Sigma\zeta_1 Z = 4.5 \times 10^8$ Pa·s m^{-1} (where $Z = 919$ is the degree of polymerization of the tethered chains), still 50 times smaller than the value observed. Clearly the simple models based on segmental friction are not consistent with our results. Hence, even with thick layers friction is enhanced by the chain pullout effects described by Ajdari, Rubinstein, and co-workers (*12*, *13*).

REFERENCES AND NOTES

1. A. I. Bailey, *J. Appl. Phys.* **32**, 1407 (1961).
2. B. J. Briscoe and D. C. B. Evans, *Proc. R. Soc. London Ser. A* **380**, 389 (1982).
3. S. J. Hirz, A. M. Homola, G. Hadziioannou, C. W. Frank, *Langmuir* **8**, 328 (1992).
4. M. L. Gee, P. M. McGuiggan, J. N. Israelachvili, A. M. Homola, *J. Chem. Phys.* **93**, 1895 (1990).
5. A. M. Homola, J. N. Israelachvili, M. L. Gee, P. M. McGuiggan, *J. Tribol.* **111**, 675 (1989).
6. J. Van Alsten and S. Granick, *Macromolecules* **23**, 4856 (1990).
7. A. D. Roberts and D. Tabor, *Proc. R. Soc. London Ser. A* **325**, 323 (1971).
8. S. C. Richards and A. D. Roberts, *J. Phys. D* **25**, A76 (1992).
9. M. Barquins, *Mater. Sci. Eng.* **73**, 45 (1985).
10. M. K. Chaudhury and M. J. Owen, *Langmuir* **9**, 29 (1993).
11. F. Brochard and P. G. de Gennes, *ibid.* **8**, 3033 (1992).
12. A. Ajdari *et al.*, *Physica A*, in press.
13. M. Rubinstein, A. Ajdari, L. Leibler, F. Brochard-Wyart, P.-G. de Gennes, *C.R. Acad. Sci. Paris Série II* **316**, 317 (1993).
14. K. B. Migler, H. Hervet, L. Leger, *Phys. Rev. Lett.* **70**, 287 (1993).
15. C. Creton, H. R. Brown, K. R. Shull, unpublished results.
16. M. K. Chaudhury and G. M. Whitesides, *Science* **255**, 1230 (1992).
17. K. P. O'Connor and T. C. M. McLeish, *Macromolecules* **26**, 7322 (1993).
18. J. M. Deutsch, private communication.
19. J. D. Ferry, *Viscoelastic Properties of Polymers* (Wiley, New York, 1980).

20. The diblock copolymer was synthesized by Y. Gallot and supplied by J. Koberstein; the XPS work was done by D. Miller; the contact angles were measured by W. Hu; and the end-reactive polystyrene was synthesized by K. Shull. I have benefited from discussions with E. J. Kramer and M. Chaudhury.

29 October 1993; accepted 26 January 1994

Differential Adhesion of Cells to Enantiomorphous Crystal Surfaces

Dorit Hanein, Benjamin Geiger, Lia Addadi

Interactions during cell adhesion to external surfaces may reach the level of discrimination of molecular chirality. Cultured epithelial cells interact differently with the {011} faces of the (*R,R*) and (*S,S*) calcium tartrate tetrahydrate crystals. In a modified version of the classical Pasteur experiment, the enantiomorphous crystals were sorted out from a 1:1 mixture by the selective adhesion of cells to the (*R,R*) crystals. This stereospecificity results from molecular recognition between chiral components on the cell surface and the structured crystal surface. Crystals may allow experimental differentiation between distinct stages in cell substrate contacts, providing mechanistic information not readily attainable on conventional heterogeneous surfaces.

Adhesion to exogenous surfaces has profound effects on the structure and behavior of cells, especially of anchorage-dependent cells (*1*). Cell substrate adhesion is commonly viewed as a molecularly complex and diversified multistage process, which includes cell attachment and spreading (*2*), focal adhesion formation, extracellular matrix deposition, and rearrangement (*3*). In general, cell attachment to and spreading on surfaces may occur through two distinct but highly interdependent mechanisms: specific binding mediated by adhesive extracellular matrix proteins and direct association with the underlying solid surface (*4*). The former interactions occur through specific proteins such as fibronectin, vitronectin, and surface integrin receptors. However, little is known about the nature of direct interactions with the substrate.

To address this issue, it is helpful to use substrates that are homogeneous and structurally defined at the molecular level. Specific molecular and organizational parameters that cannot be defined on heterogeneous substrates such as glass and tissue culture plastics can be thus characterized. We examined the manner in which crystals operate as substrates for cell adhesion.

D. Hanein and L. Addadi, Department of Structural Biology, Weizmann Institute of Science, 76100 Rehovot, Israel.
B. Geiger, Department of Chemical Immunology, Weizmann Institute of Science, 76100 Rehovot, Israel.

The detailed molecular and structural information available for these homogeneous and repetitive rigid surfaces offers means of identifying the molecular attributes that directly influence the interactions occurring in the cell substrate recognition process.

In a previous study, we found that two structurally distinct faces of the same crystal, calcium (*R,R*)-tartrate tetrahydrate, differ greatly in their capacity to serve as adhesive substrates (*5*). These prismatic crystals are delimited by two different face types, denoted {011} and {101} (*6*), which are by definition chemically equivalent, but differ in their structural organization (*7, 8*). Within 10 min after plating, a massive attachment of epithelial cells (*Xenopus laevis* kidney A6 cell line) occurred on the {011} faces. This binding is presumably independent of exogenous proteins as it is not affected by Arg-Gly-Asp (RGD) peptides (*9*) or the presence of serum in the medium. In contrast, cell adhesion to the {101} faces is relatively slow (>24 hours), is promoted by serum proteins, and can be inhibited by RGD peptides. The rate of adhesion to the {011} faces is faster than that observed on "conventional" tissue culture substrates, whereas the binding to the {101} faces is much slower.

The differential behavior of the cells toward the two distinct faces suggests that adhesive interactions are sensitive to surface organizational variations on the angstrom scale. This means that an approaching cell "senses" only the groups directly exposed at the surface or within the first few (3 to 4) angstroms (*5*). However, it remained unclear whether direct recognition and cell attachment are determined by the general chemical nature (or chemical potential) of the surface or by its specific structural and molecular organization. To address this question, we exploited the chiral nature of the tartrate molecule and investigated the adhesive response of A6 cells to the enantiomorphous crystals of calcium (*R,R*)- and (*S,S*)-tartrate tetrahydrate crystals. These two crystals have exactly the same intermolecular lattice organization, but both the component molecules and the structure are mirror images of each other (Fig. 1). The distribution and the relative orientation of the molecules on the expressed surfaces are identical.

Light and electron microscopic observations indicated that cells seeded and grown on regular culture dishes, in a complete medium saturated with respect to each of the two enantiomers in the solution, showed normal morphology and growth characteristics indistinguishable from those of cells cultured in complete medium (*10*). These observations indicate that both enantiomers of tartrate, in solution, have no apparent effect on adhesion and growth on conventional tissue culture surfaces. Cells were then seeded in dishes containing saturated medium and crystals of either one of the enantiomorphs. The manner in which they attached to the crystals was determined by light and scanning electron microscopy. After 10 min of incubation, the {011} faces of the (*R,R*) crystal form were densely covered by adherent A6 cells (Fig. 2A), whereas almost no cells were observed on the equivalent faces of (*S,S*) crystals (Fig. 2B). Both the extent and kinetics of the "slow" cell adhesion to the {101} faces of the two enantiomeric crystals, which was apparent ~24 hours after plating, were identical (Fig. 2, C and D).

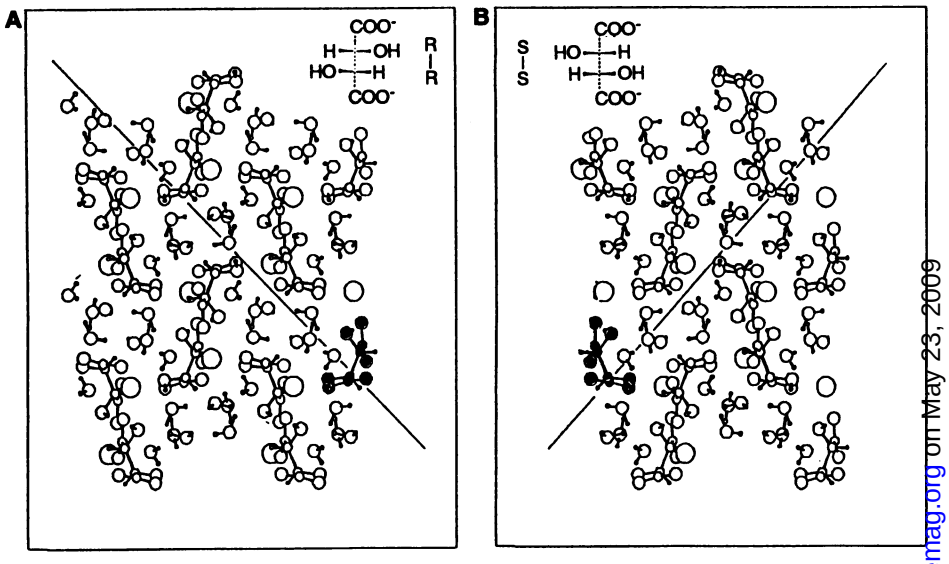

Fig. 1. Computer graphic representation of the packing arrangement of (**A**) calcium (*R,R*)-tartrate tetrahydrate and (**B**) calcium (*S,S*)-tartrate tetrahydrate crystals viewed on the (100) plane. The {011} (*6*) planes are viewed edge-on (bold line), showing the molecules exposed at the crystal surface. The circles, in decreasing size, represent Ca, O, C, and H. The two faces have the same intermolecular lattice organization but are the mirror image of each other. Calcium tartrate tetrahydrate crystallizes in the orthorhombic space group $P2_12_12_1$, with lattice parameters a = 9.152 Å, b = 10.504 Å, c = 9.554 Å, and Z = 4. The {011} faces are covered by bound water molecules organized in parallel rows, giving rise to channels and ridges on the surface in a direction parallel to the a axis. The tartrate molecule (filled circles) exposes only hydroxyl groups and one carboxylate group at the surface; the carboxylate group has an oblique orientation (*5, 8*).

Table 1. The short-term (1-hour) adhesive response of different cell types to calcium (*R,R*)- and (*S,S*)-tartrate tetrahydrate crystals in the absence or in the presence of RGD peptide. The results of the experiments performed in the presence of RGD peptide are reported within parentheses. The cells used were A6 (kidney, *Xenopus laevis*, epithelial-like, ATCC CCL 102), MDCK (kidney, canine, epithelial-like, ATCC CCL 34), MCF7 (breast adenocarcinoma, human, epithelial-like, ATCC HTB 22), RAT1 (spontaneously immortalized rat embryo fibroblast), and CEF (chicken embryo fibroblast, primary). The symbols 0, +, ++, and +++ relate to the number of cells observed on the crystals. The symbols in bold highlight stereospecific, direct cell attachment. Neither crystal type provided compatible surfaces for CEF cell adhesion. The MCF7 cells were insensitive to both structural and chiral parameters of the substrate as well as to presence of the RGD peptide. Chiral recognition through an RGD-independent mechanism was observed in A6, MDCK, and RAT1 cells. All of the cell types were cultured as described in Fig. 2 at 37°C, except the A6 cells, which were incubated at 28°C. In the experiments with RGD peptide, 50 μg/ml of the synthetic peptide Gly-Arg-Gly-Asp-Ser (Bachem, Switzerland) were added to the complete medium before cell seeding. Crystallization, cell seeding, fixation, and electron microscopy monitoring were performed as described in Fig. 2.

Cells	Crystals							
	Calcium (*R,R*)-tartrate				Calcium (*S,S*)-tartrate			
	{011} faces		{101} faces		{011} faces		{101} faces	
A6	+++	(+++)	0	(0)	0	(0)	0	(0)
MDCK	++	(++)	++	(+)	++	(+)	++	(+)
MCF7	+	(+)	+	(+)	+	(+)	+	(+)
RAT1	0	(0)	0	(0)	+	(+)	++	(+)
CEF	0	(0)	0	(0)	0	(0)	0	(0)

The stereospecificity of the adhesion to the {011} faces of the (*R,R*) crystals was unambiguously established by the following experiment. Cells were plated on an artificial homogeneous 1:1 mixture (60 mg) of the enantiomorphous (*R,R*) and (*S,S*) crystals. The cells were fixed 10 min after seeding to enhance their contrast (*11*). The crystals on which cells were observed under a stereomicroscope were hand picked and separated. The separated fraction of cell-coated crystals (16.2 mg) was dissolved (in 1 ml of 1 M HCl). The measured optical activity of the solution ($\alpha = +0.10$, $[\alpha]_D = +6.30$) corresponded to (*R,R*) tartaric acid of 86.2% enantiomeric purity. The experiment was repeated, yielding $[\alpha]_D = +6.06$, corresponding to (*R,R*) tartaric acid of 83% enantiomeric purity (*11*). This sorting experiment is reminiscent of that performed by Pasteur in 1848 whereby sodium ammonium tartrate crystals were sorted manually according to their distinct hemihedral morphology (*12*). Because calcium tartrate tetrahydrate crystals do not develop hemihedral faces and are indistinguishable morphologically, the results of this experiment depended solely on the ability of the cells to distinguish between the {011} faces of the two enantiomers. The results indicate that these cells are able to differentiate between structural organizational motifs, even down to the level of molecular chirality.

To determine whether the stereospecific recognition manifested by A6 cells is a unique property of this cell type, we checked the adhesive responses of various cultured cells: MCF7, MDCK, RAT1, and CEF (Table 1). Each cell type was seeded on the two enantiomorphs of calcium (*R,R*)- or (*S,S*)-tartrate tetrahydrate crystals separately, and their short-term adhesive responses were determined. The cells were seeded onto the crystals in saturated complete medium (*10*), with or without RGD peptide, to distinguish between RGD-dependent and -independent adhesion mechanisms. The results (Table 1) indicate that the stereospecific adhesion is RGD-independent and varies among different cell types. For example, the chiral preference observed in RAT1 is opposite to that of A6 and MDCK cells. In MDCK cells, direct, stereospecific binding is masked by RGD-dependent adhesion (Table 1). Although the identity of the specific elements involved in the recognition process remains to be determined, these results suggest that recognition depends on chiral molecules (or macromolecules) binding to defined molecular moieties on either (*R,R*) or (*S,S*) tartrate molecules, exposed at the {011} crystal surface.

Adhesion may be viewed as a biphasic process composed of "nucleation" and "extension" stages (*2*). In molecular terms, the nucleation phase may involve relatively rapid local surface interaction. The extension stage requires a major organization of the cytoskeleton, leading to gross changes in cell shape and recruitment of specific adhesion receptors to these sites (*13*). In conventional adhesive substrates, the molecular heterogeneity (*14*) of the surface presumably provides a balanced variety of binding sites for both stages, rendering it difficult to distinguish between the two. Our experiments provide a means of experimentally distinguishing between the nucleation and extension stages. Furthermore, the crystals present an artificially dense array of selected chemical moieties as a repetitive and homogeneous lattice, thus amplifying interactions that are probably rare (sparse) on physiological substrates. It is tempting to speculate that the massive rapid adhesion to the {011} faces represents an excessive, chirally restricted nucleation event that is not followed by normal cell spreading and development of focal adhesions, whereas adhesion to the {101} faces is characterized by poor nucleation, followed by slow, yet effective, development of stable adhesions.

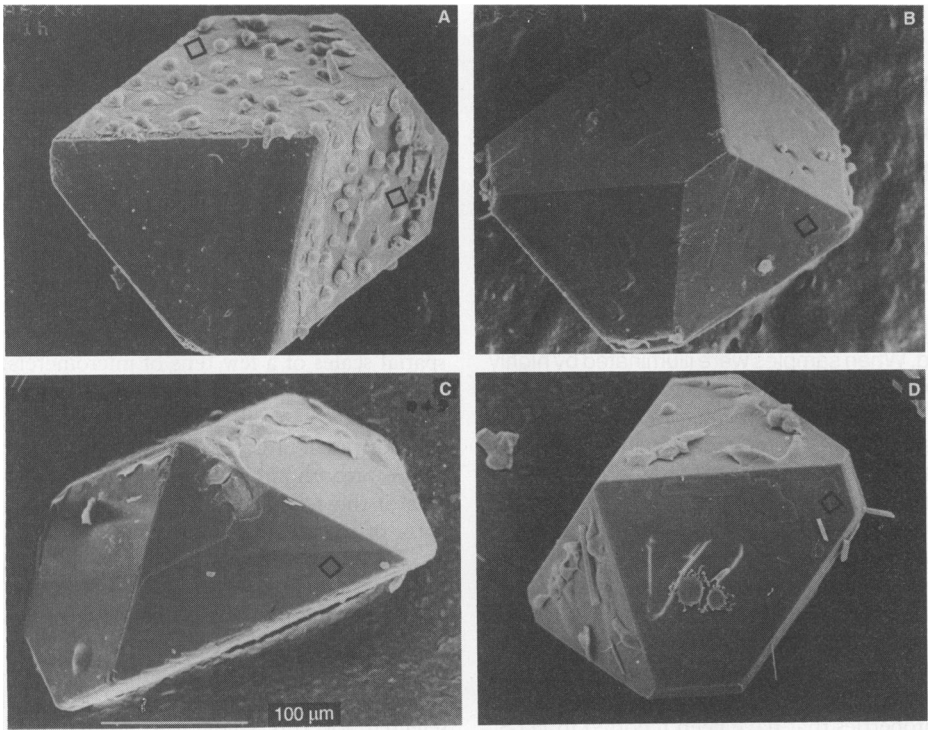

Fig. 2. Scanning electron micrographs of cultured *Xenopus laevis* kidney epithelial A6 cells plated on calcium tartrate tetrahydrate crystals. The short-term adhesive response (10 min) is shown for (**A**) the (*R,R*) form and (**B**) the (*S,S*) form. The long-term adhesive response (24 hours) for (**C**) the (*R,R*) form and (**D**) the (*S,S*) form. The {011} faces are marked by the bold squares. For each crystal system, optimal conditions for crystallization from aqueous solution were determined, ensuring that the crystals were well-formed, homogeneous, and reproducible with respect to morphology and size. All crystallization experiments were carried out at room temperature. Crystallization conditions for calcium (*R,R*)-tartrate tetrahydrate crystals: 30 ml of 40 mM sodium hydrogen tartrate was mixed with 30 ml of 43 mM $CaCl_2 \cdot 2H_2O$ at pH 6.5 and transferred to 3.5-cm cell culture dishes (Falcon). Crystallization conditions for calcium (*S,S*)-tartrate tetrahydrate crystals were the same as for the (*R,R*) form except for the use of (*S,S*) tartrate. Typically, crystals of ~1-mm size formed within 1 day. Routinely, cells were cultured at 28°C in Dulbecco's minimum essential medium, supplemented with 10% fetal bovine serum (complete medium), on the same culture dishes in which the crystals were previously grown, still attached to the dish (*5*). To avoid crystal dissolution, we saturated all culture, fixation, and washing solutions with respect to the particular crystal used (saturated complete medium). Cell fixation was performed with 2% glutaraldehyde in 0.1 M cacodylate buffer, pH 7.2, for 30 min. The dishes were rinsed twice and postfixed for 30 min with 1% osmium tetroxide in 0.1 M cacodylate buffer. After a further rinse, the crystals were detached from the dishes, transferred to Microporous Spec Cap (Spi Supplies), dehydrated with ethanol, and critical-point dried with CO_2 (Autosamdri-810, Tuosimis). The crystals were placed on carbon-coated stubs and sputter coated with gold. The specimens were examined at an accelerating voltage of 10 to 15 kV (JEOL 6400 scanning electron microscope). The identification of crystal faces was performed as previously reported (*5*).

REFERENCES AND NOTES

1. J. M. Vasiliev and I. M. Gelfand, *Neoplastic and Normal Cells in Culture*, vol. 8 of the Developmental and Cell Biology Series, D. R. Newth and J. G. Torrey, Eds. (Cambridge Univ. Press, Cambridge, 1981), pp. 19–174.
2. F. Grinnell and D. G. Hays, *Exp. Cell Res.* **116**, 275 (1978).
3. K. Burridge, K. Fath, T. Kelly, G. Nuckolls, C.

Turner, *Annu. Rev. Cell Biol.* **4**, 487 (1988); B. Geiger, T. Volk, T. Volberg, R. Bendori, *J. Cell Sci. Suppl.* **8**, 251 (1987).
4. R. O. Hynes, *Cell* **69**, 11 (1992).
5. D. Hanein, H. Sabanay, L. Addadi, B. Geiger, *J. Cell Sci.* **104**, 257 (1993).
6. Crystal faces are described by a set of indices (*hkl*) that unequivocally define the orientation of the face relative to the crystallographic axes *a*, *b*, and *c* of the structure. The notation {*h,k,l*}, such as {011}, includes a set of faces—(01$\bar{1}$), (0$\bar{1}$1), and (0$\bar{1}\bar{1}$)—that are identical to (011) because they are related to it by the symmetry of these crystals.
7. G. K. Ambady, *Acta Crystallogr. Sect. B* **24**, 1548 (1968).
8. D. Hanein, B. Geiger, L. Addadi, *Langmuir* **9**, 1058 (1993).
9. Many adhesive proteins present in the extracellular matrices and in the blood contain the sequence RGD as their major cell recognition site. The RGD sequences of each of the adhesive proteins are recognized by at least one member of structurally related receptors of the integrin superfamily. The synthetic peptides, containing the RGD sequence, inhibit extracellular matrix-mediated cell adhesion.
10. Routinely, cell growth was performed in the presence of 10% fetal bovine serum, saturated with respect to the particular crystal used (saturated complete medium).
11. A6 cells were seeded on a mixture of calcium (*S,S*)- and (*R,R*)-tartrate tetrahydrate crystals in 5.5-cm Falcon (Plymouth, United Kingdom) culture dishes. The crystals were homogeneous in size, and the starting weight of each fraction was ~60.0 mg. After 10 min, the cells were fixed with 2% glutaraldehyde in 0.1 M cacodylate buffer, pH 7.2, containing 5 mM $CaCl_2$. The dishes were rinsed four times, postfixed with 1% osmium tetroxide in the same buffer, and dried. The fixation kept the cells in situ and enhanced contrast. The crystals on which cells were observed were manually separated from others under a Zeiss (Oberkochen, Germany) stereomicroscope, 80× magnification. The selected cell-coated crystals (16.2 mg) were dissolved in 1 ml of 1 M HCl, and the optical activity of the solution was measured with a Perkin-Elmer 141 polarimeter. The optical activity of the solution was α = +0.104, $[\alpha]_D$ = +6.30, corresponding to (*R,R*) tartaric acid of 86.2% enantiomeric purity {$[\alpha]_D$ = +7.3 for pure calcium (*R,R*)-tartrate tetrahydrate in 1 M HCl}. The experiment was repeated, yielding $[\alpha]_D$ = +6.06, corresponding to (*R,R*) tartaric acid of 83% enantiomeric purity.
12. L. Pasteur, *Ann. Chim. Phys.* **xxiv**, 442 (1848).
13. B. Geiger, D. Salomon, M. Takeichi, R. O. Hynes, *J. Cell Sci.* **103**, 943 (1992).
14. A. S. G. Curtis and P. Clark, *Crit. Rev. Biocompat.* **5**, 343 (1990).
15. We thank K. Ben-Ari, a high school student who performed her final class project in our laboratory, for motivating with her presence the execution of this work. We thank our colleagues M. Lahav and S. Weiner for critically reading the manuscript. B.G. holds the E. Neter Chair for Cell and Tumor Biology. L.A. is incumbent of the Patrick E. Gorman Chair of Biological Ultrastructure. This work is supported in part by the Kimmelman Center for Structural Biology, a grant from the Minerva Foundation, Munich, Germany (B.G.), and the Anniversary Fund of the Austrian National Bank.

18 October 1993; accepted 12 January 1994

Direct Observation of Microscopic Inhomogeneities with Energy-Dispersive Diffraction of Synchrotron-Produced X-rays

E. F. Skelton, A. R. Drews, M. S. Osofsky, S. B. Qadri, J. Z. Hu, T. A. Vanderah,* J. L. Peng, R. L. Greene

Evidence of structural inhomogeneities in two high–transition-temperature superconductors, $YBa_2Cu_3O_{7-\delta}$ and $Nd_{2-x}Ce_xCuO_{4-y}$, is presented. When samples were illuminated by highly collimated x-rays produced on a synchrotron wiggler, small changes in the lattice were detected over a spatial scale of 10 micrometers. These changes are interpreted as evidence of variations in the oxygen content in one case and in the cerium content in the other; both affect the superconducting properties. The existence of such structural inhomogeneities brings into question whether exotic experimental results obtained from superconducting materials with high transition temperatures actually reflect intrinsic properties.

High-temperature superconductors (HTS) still present many mysteries in both their chemical properties and the mechanism of superconductivity. One of the few characteristics that is universally accepted is that their coherence lengths, ξ, are short (on the order of tens of angstroms). Because ξ is the decay distance of the superconducting order parameter, sample inhomogeneities, even in single crystals, strongly affect the measured superconductive properties of the system. These inhomogeneities are undoubtedly the source of many of the unusual properties that have been reported in HTS. In this report, we present direct structural evidence of microscopic oxygen and cation inhomogeneities in crystals of HTS.

Standard diffraction techniques with conventional x-ray sources are the classic method for obtaining structural information. This information is limited to a surface region of the sample, as defined by the penetration depth of the radiation. This depth varies with photon energy and the atomic number of the elements in the sample. Typical skin depths are on the order of a few micrometers. Spot sizes are determined, in part, by the degree to which the radiation from an x-ray generator can be collimated, while retaining an adequate number of photons in the beam to perform the measurement. Typical beam diameters are on the order of millimeters. Neutron diffraction typically requires samples of millimeter dimensions or larger, and although electron beam cross sections can be reduced to less than a micrometer, their penetrating power is limited. However, with the use of high energy photons from a synchrotron wiggler, with its concomitant low angular dispersion, materials can be probed roughly two orders of magnitude deeper with x-ray beams that are <100 μm^2 in cross-sectional area. Using such an arrangement, we have detected small compositional variances on spatial scales of a few tens of micrometers.

Experiments were performed on a $YBa_2Cu_3O_{7-\delta}$ single crystal to determine compositional uniformity. The *c* axis length of the orthorhombic unit cell of bulk samples of these compounds is a reliable indicator of the oxygen content, $7 - \delta$ (*1*)

$$7 - \delta = 74.49 - 5.787\,c \qquad (1)$$

where *c* is in angstroms. The $YBa_2Cu_3O_{7-\delta}$ crystals were grown from an off-stoichiometric flux in a zirconia crucible as described in detail elsewhere (*1*). The crystal selected for this study was mechanically detwinned (*2*). Optical microscopic analysis after detwinning showed the crystal to be almost entirely twin-free, and x-ray studies on a four-circle diffractometer showed no evidence of twinning. On the basis of ac-susceptibility measurements, the transition temperature T_c had an onset of 93 K and a width less than 0.5 K.

The crystal was in the approximate shape of a rectangular solid, with dimensions 470 μm by 340 μm by 75 μm. The [0,0,ℓ] reciprocal lattice vector was normal to the largest face, and the longest edge was approximately parallel to the *b* axis. The crystal was mounted on an ω,χ circle (angles ω and χ measure the rotational motion of the sample about vertical and horizontal axes, respectively), contained on an *xyz*-translation stage on beamline X17C at the National Synchrotron Light Source (NSLS), Brookhaven National Laboratory, and was

E. F. Skelton, A. R. Drews, M. S. Osofsky, S. B. Qadri, Condensed Matter and Radiation Sciences Division and Materials Science and Technology Division, Naval Research Laboratory, Washington, DC 20375–5000, USA.
J. Z. Hu, Geophysical Laboratory and Center for High Pressure Research, Carnegie Institution of Washington, Washington, DC 20015–1305, USA.
T. A. Vanderah, Chemistry Division, Research Department, Naval Air Warfare Center, Weapons Division, China Lake, CA 93555, USA.
J. L. Peng and R. L. Greene, Center for Superconductivity Research, Department of Physics, University of Maryland, College Park, MD 20742, USA.
*Present address: Ceramics Division National Institute of Standards and Technology, Gaithersburg, MD 20882, USA.